ACCOUNTS
of chemical research

Pyramids: A Platform for Designing Multifunctional Plasmonic Particles

JEUNGHOON LEE,[†] WAREFTA HASAN,[†]
CHRISTOPHER L. STENDER,[†] AND TERI W. ODOM*[,†,‡]

[†]*Department of Chemistry,* [‡]*Department of Materials Science and Engineering, Northwestern University, 2145 Sheridan Road, Evanston, Illinois 60208*

RECEIVED ON MAY 16, 2008

CONSPECTUS

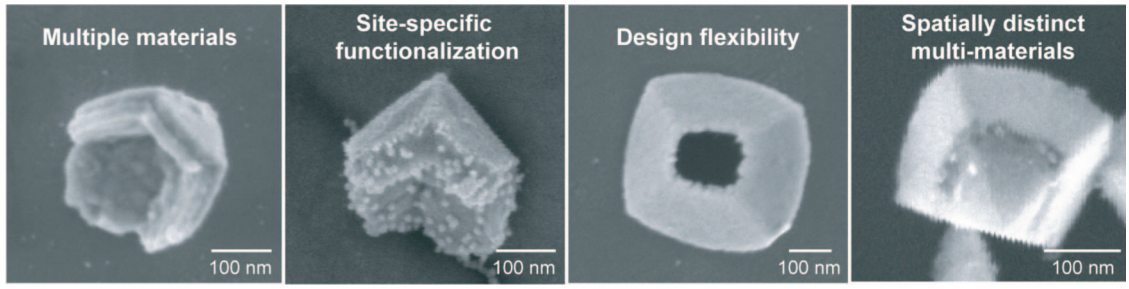

This Account explores nanofabricated pyramids, a new class of nanoparticles with tunable optical properties at visible and near-infrared wavelengths. This system is ideally suited for designing multifunctional plasmonic materials for use in diagnostics, imaging, sensing, and therapeutics. The nanofabrication scheme that we developed (called PEEL) for these asymmetric metal particles is extremely versatile and offers several advantages over synthetic methodologies.

The PEEL approach yields pyramids with variable sizes, thicknesses, and multimetal compositions, as well as blunt or ultrasharp tips or no tips. In addition, we have prepared pyramids with site-specific chemical and biological functionality on different portions of the pyramids. This is an important design feature for biological applications, as suggested by the generation of amphiphilic gold pyramids functionalized with alkanethiols on the hydrophobic portions and DNA on the hydrophilic portions.

The optical characteristics of these pyramids depend on particle orientation, wavevector direction, and polarization direction and can be tuned. Using the multipolar surface plasmon resonances of large (>250 nm) pyramids, imaging and spectral identification of pyramid orientation in condensed media was possible. We were also able to direct pyramids to assemble into one- and two-dimensional arrays with interesting optical properties. Furthermore, modification of the PEEL fabrication scheme allowed the production of multimaterial pyramidal structures with complex attributes, highlighting the power of this platform for exacting nanometer-scale control over particle structure and composition.

Introduction

Plasmonics, the science and application of noble metal structures interacting with light, has received significant attention recently because of three cooperative effects to *make*, *measure*, and *model*.[1] Advances in nanoparticle (NP) synthesis and fabrication, innovations in novel analytical tools and measurements, and clever theoretical modeling have been drivers for new discoveries. Noble metal NPs support localized surface plasmon (LSP) resonances, which can be tuned by controlling particle size, shape, and materials composition and surrounding dielectric environment.[2−4] The first plasmonic NPs to be synthesized and characterized were gold and silver colloids.[5] The optical properties of plasmonic particles are determined by relative contributions of absorption and scattering of light (extinction = absorption + scattering). Small metal particles (overall sizes <50 nm) are dominated by the former process, while larger

Published on the Web 09/20/2008 www.pubs.acs.org/acr
10.1021/ar800126p CCC: $40.75

particles (>100 nm) are dominated by the latter.[6,7] Furthermore, small spherical particles support single LSP resonances that are dipolar in character, and their optical response can be described well by the lowest order term in Mie theory.[6] Particle sizes of several hundred nanometers exhibit multiple LSP resonances[8,9] that correspond to higher order plasmon modes.[10,11]

Because plasmonic NPs exhibit intense localized electric fields, they have been exploited for enhancing and detecting weak processes. Examples include chemical and biological detection[12−16] and surface-enhanced Raman spectroscopy (SERS).[17,18] Besides these diagnostic applications, plasmonic particles are becoming increasingly important in biomedical imaging and therapeutics because (1) they have large extinction cross-sections (10^4-10^5 times for 30-nm gold or silver NPs compared with fluorescent dyes[7]) and do not photobleach,[19] (2) they exhibit plasmon resonances at near-infrared (NIR) wavelengths (800−1300 nm), which is the biological window where tissue is relatively transparent,[20,21] (3) gold and silver NPs are not cytotoxic (up to a few micromolar),[22,23] and (4) the light absorbed and scattered by metal NPs can be converted to heat.[24,25]

Preparation of Anisotropic Metal Nanoparticles

Typically, plasmonic nanoparticles are synthesized using solution techniques that involve the reduction of metal salts in the presence of surfactants. An extensive overview of the different conditions and outcomes has been published elsewhere.[26,27] Particles with anisotropic shapes, including rods,[9,21] cubes,[28] cages,[29] shells,[20] prisms,[30] stars,[31] and octahedra,[32] have been made; such shapes usually have a high degree of *symmetry*. Solution synthesis offers a straightforward and relatively inexpensive way to scale the production of anisotropic metal particles. There are several challenges, however, in synthesizing multifunctional plasmonic NPs. First, to prepare particles consisting of two or more metals, elaborate synthetic schemes are necessary.[4,33] Second, because particle surfaces are stabilized with surfactant molecules, ligand displacement reactions are required to achieve desirable functionalities. Third, although specific locations of NPs can be differentially modified, the procedures typically require the use of solid-phase templates[34,35] or assemblies of mixed ligands,[36] which adds additional steps to the process. To access metal NPs with anisotropic as well as *asymmetric* shapes and to create them from a wider variety of materials more readily, alternative strategies are critical.

Nanofabrication offers a top-down approach for preparing highly anisotropic and asymmetric metal nanostructures with a high level of control over size and shape. Fabrication techniques are especially suited to generate particles with overall sizes that exceed 100 nm. Serial patterning techniques such as electron beam lithography can generate two-dimensional (2D) structures with arbitrary sizes and shapes,[37,38] although the throughput is very low. Besides direct-write methods, templates have been the primary method to produce particles with anisotropic shapes. Isolated submicrometer spheres and close-packed sphere arrays have acted as templates onto which metals were deposited to obtain particles with crescent-like shapes[39,40] and truncated triangular prisms.[41] Anodized aluminum oxide membranes are another widely used template for producing nanorods as long as 10 μm.[42] Etched silicon templates and nanohole masks have been used to create pyramidal shells.[43,44]

In addition, fabrication methods offer several general advantages over chemical ones. First, different materials compositions can easily be prepared in particles using sequential deposition steps. Second, because the surfaces of as-prepared NPs are surfactant-free, they can be directly functionalized with thiolated biological and chemical moieties. Third, NPs can be organized into periodic arrays with well-defined interparticle orientations. In this Account, we review a new class of asymmetric metal particles, nanofabricated pyramids, that are an ideal platform for designing multifunctional plasmonic materials. The fabrication method is versatile and can generate pyramids with different sizes and thicknesses, with blunt, ultrasharp, or no tips, and with different materials combinations. Because of their relatively large sizes (>150 nm) and anisotropic shape, the pyramids exhibit tunable optical properties at visible and NIR wavelengths that depend on particle orientation, wavevector direction, and polarization direction. Such unique geometrical and optical characteristics make possible new applications in imaging and sensing.

A New Plasmonic Platform: Pyramidal Particles

Size, Shape, and Materials Control. We have developed a nanofabrication approach, PEEL (a procedure consisting of phase-shifting photolithography (PSP), etching, E-beam deposition, and lift-off), which can generate free-standing pyramidal structures with diameters ranging from 80 to 500 nm and tips with radii of curvature as small as 2 nm.[43] The nanofabricated pyramids are highly uniform in size and shape because they are formed by templating against an etched single-crystal Si(100) wafer.[45] Figure 1 outlines how different steps in the PEEL process can result in a wide range of tunability regarding the size, shape, and materials of the pyramids. First, PSP

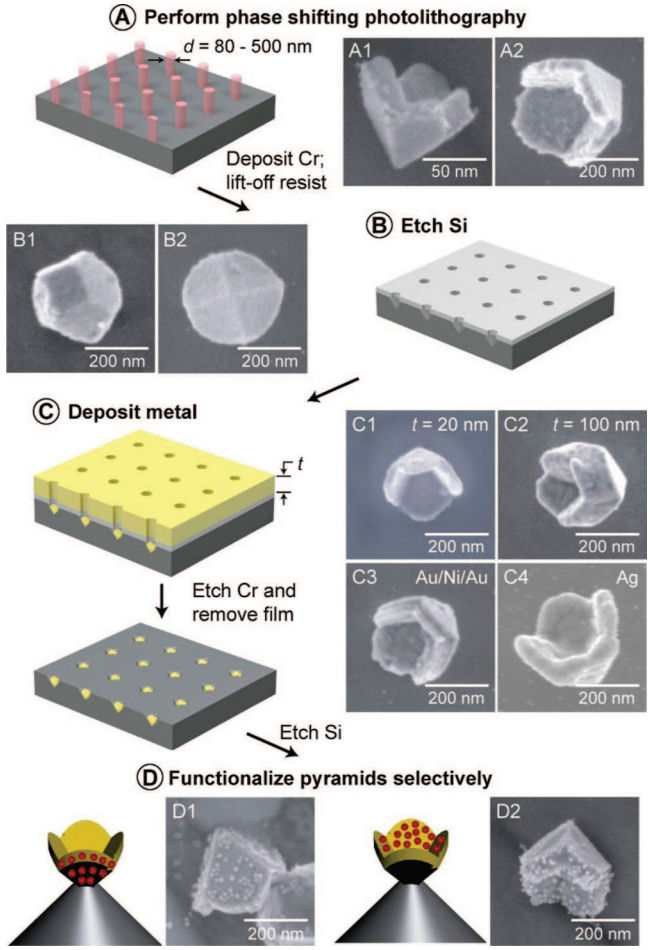

FIGURE 1. Scheme representing the broad tunability range of structural, materials, and chemical parameters of the nanofabricated pyramid system.

is used to generate arrays of circular posts in positive-tone photoresist (step A); the diameters (*d*) determine the size of the base of the pyramids. A thin film of Cr is then deposited onto the substrate and lifted-off to produce small, circular holes. Depending on how long the Cr/Si substrate is anisotropically etched (step B), the pyramids will either have sharp tips or flat (and blunt) tips. Different materials can then be deposited into the etched pyramidal pits (step C); here is where the thickness (*t*), materials composition, and multilayered structure of the pyramids are determined. Next, the Cr layer is etched to reveal pyramids embedded in the Si substrate, which is then partially etched so that the inner and outer surfaces can be differentially modified with molecules having different functionalities (step D). The pyramids can be dispersed into solution by sonication.

Selective Functionalization of Pyramid Faces. The ability to differentially modify specific portions of NPs is important for designing hierarchical, multifunctional structures for therapeutic and diagnostic applications. PEEL provides two

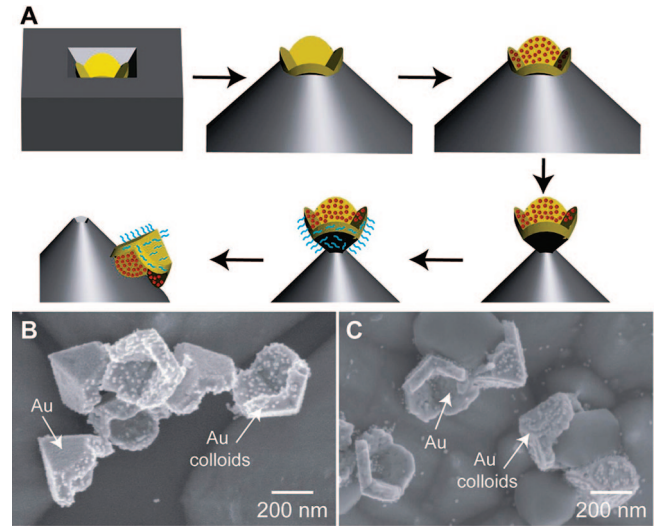

FIGURE 2. (A) Procedure for selective functionalization of gold pyramids patterned on a silicon template and SEM images of pyramids selectively functionalized with DNA and hybridized with DNA-modified 13 nm Au colloids on their (B) inner and (C) outer surfaces. Reproduced with permission from ref 45. Copyright 2007 American Chemical Society.

complementary routes to control the placement of molecules on the pyramid faces: (1) selective functionalization of single-material pyramids on the patterned silicon template or (2) functionalization of multimaterial pyramids in solution. In the first approach, as part of their fabrication procedure (Figure 1, step B), the pyramids are embedded in the Si substrate with only their inner surface exposed. Here the inner surfaces of the pyramids can be decorated with thiolated molecules. Further etching of the substrate exposes the outer faces of the pyramids, and modification with another type of thiolated molecule can result in differentially functionalized particles. Figure 2 shows how gold pyramids with amphiphilic character can be prepared, where the hydrophilic portions were single-stranded DNA (visualized by gold colloids modified with the cDNA strand) and the hydrophobic portions were alkanethiols.[45] In the second approach, after multimaterial pyramids are dispersed in solution, differential modification can be achieved using ligands with affinity to only one of the metals. As shown in Figure 3, pyramids whose outer shell was gold and inner shell was nickel (Au/Ni pyramids) and whose outer shell was nickel and inner shell was gold (Ni/Au) only had thiolated DNA attached to the gold surfaces.[46]

Imaging Capabilities and Spectroscopic Properties of Single Pyramids

We have used dark field (DF) microscopy and spectroscopy to study the optical properties of the individual pyramids. White light incident from a DF condenser at high angles (ca. 53°−71°) is scattered by pyramids supported on a substrate,

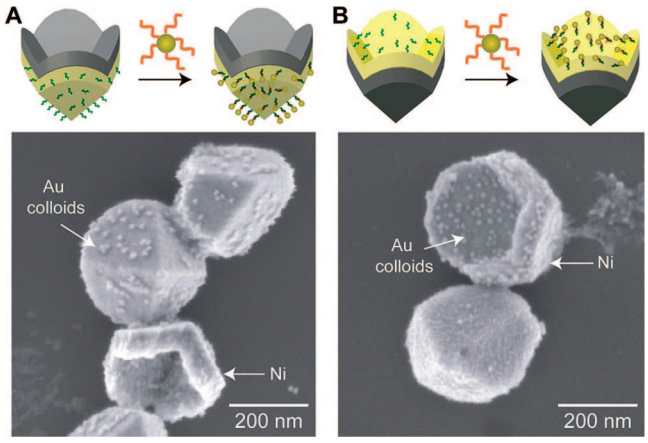

FIGURE 3. Schemes and SEM images of bimaterial pyramids selectively functionalized in solution: (A) Au/Ni pyramids; (B) Ni/Au pyramids with gold colloids attached to the gold faces by DNA molecules. Reproduced from ref 46.

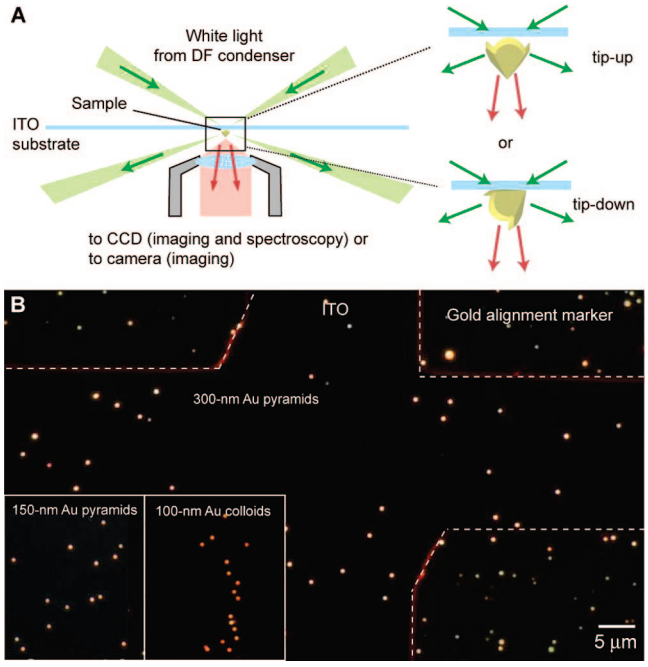

FIGURE 4. (A) Illustration of the DF microscopy and spectroscopy setup and the two different orientations of pyramids and (B) DF image of 300 nm gold pyramids, 150 nm gold pyramids, and 100 nm gold colloids on ITO/glass substrates.

collected by an objective lens, and then projected onto a CCD imaging detector or analyzed using a grating spectrometer (Figure 4A). To correlate the orientation and structure (size, shape) of the pyramidal particles with their scattering spectra, we used gold alignment markers on ITO-coated glass substrates. In this way, we carried out single-particle spectroscopy. When randomly dispersed on a flat substrate, pyramids adopt two orientations: (1) with their tips pointing away from the surface (tip-up) or (2) with their tips touching the surface (tip-down). Spectral analysis of the scattered light revealed

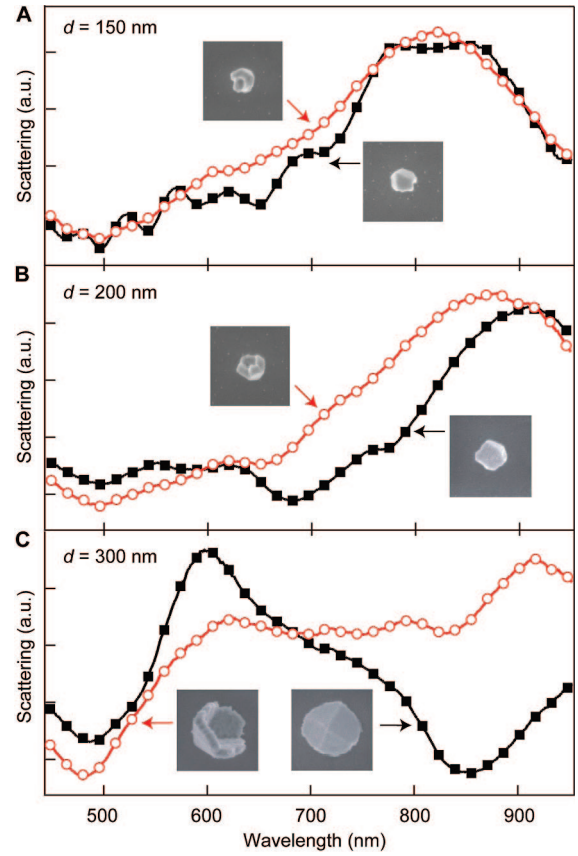

FIGURE 5. Single-particle scattering spectra of 60-nm thick gold pyramids with base diameters of (A) 150, (B) 200, and (C) 300 nm.

interesting and complex spectral features characteristic of pyramids with different diameters, orientations, and thicknesses.

Effects of Pyramid Size on Optical Properties. Figure 4B demonstrates how light scattered by gold pyramids can be imaged with high contrast compared with the optically flat substrate. Larger pyramids ($d = 300$ nm) scattered white light more strongly than smaller particles ($d = 150$ nm); in comparison, spherical 100-nm gold particles scattered red light strongly, while pyramids scattered a broader range of wavelengths. Previously, we found that 100-nm gold pyramids only supported a single dipolar resonance that occurred around 720 nm when $t = 50$ nm. The shape and location of the LSP resonance was in good agreement with discrete dipole approximation (DDA) calculations.[11] As their diameters increased from 150 to 300 nm ($t = 60$ nm), the pyramids began to develop structure in their scattering spectra that depended on both size and orientation (Figure 5). First, as the diameter of the pyramid base increased, the dipolar resonance shifted to longer wavelengths, and peaks and other structure started to emerge around 600 nm (Figure 5B,C). Second, the spectral features that are now blue-shifted relative to the dipolar resonance are more pronounced for 300 nm pyramids. Figure 5C indicates that the spectrum of tip-up pyra-

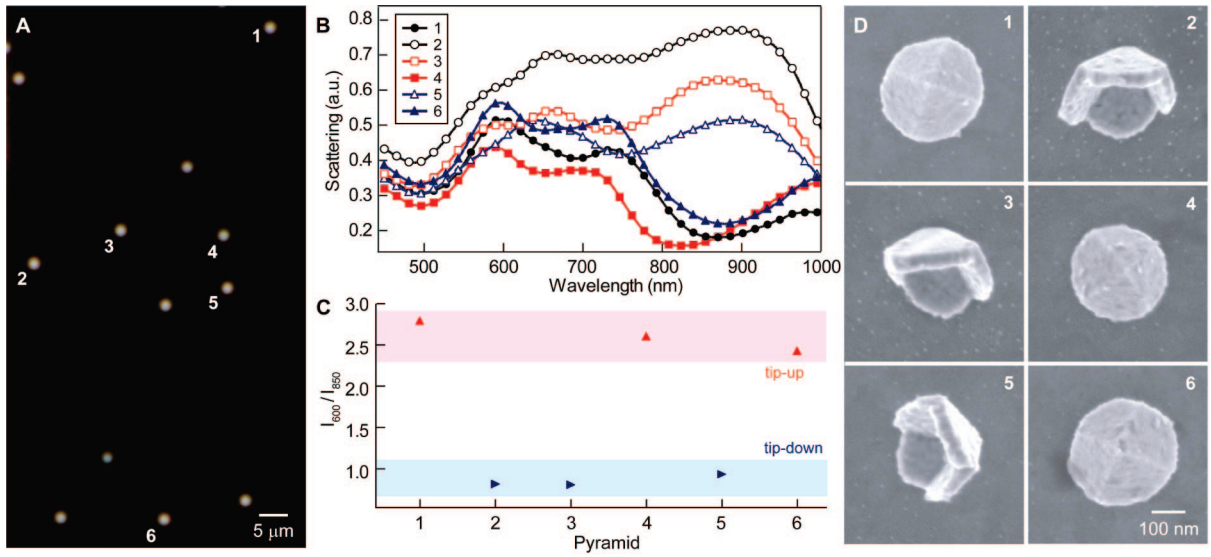

FIGURE 6. (A) DF image of individual 300 nm gold pyramids on ITO, (B) single-particle scattering spectra of pyramids indicated in panel A, (C) ratio of intensities at 600 and 850 nm of the pyramids, and (D) SEM images confirming the orientation of pyramids predicted by their spectra in panel B. Reproduced with permission from ref 45. Copyright 2007 American Chemical Society.

mids is dominated by the resonance around 600 nm, while tip-down pyramids exhibit a 600-nm peak with reduced intensity but an additional one at NIR wavelengths.

In submicrometer particles, such as triangular and rectangular prisms,[9,10,47] cylinders,[48] spherical shells,[49] and pyramidal shells,[11] multipolar excitations depend on the direction of the wavevector and the polarization vector.[50] When the particles have sizes comparable to the wavelength of incident light, their optical resonances are sensitive to the direction of excitation, and certain excitation angles can make selected resonances more pronounced.[47] For example, depending on the direction of incident light, the phase of the excitation field in asymmetric gold pyramids can vary significantly,[11] which can result in the excitation of different superpositions of multipolar resonances.[51] These effects can also be observed when the pyramids are in different orientations (i.e., the incident wavevectors are fixed but the base plane of the pyramid is at an angle), as described below.

Effects of Pyramid Orientation on Optical Properties. Large (d > 250 nm) pyramids in different orientations (tip-up and tip-down) should exhibit distinct scattering spectra. This unique characteristic of our asymmetric particles, in the absence of polarization, enables their orientation to be determined in condensed media without the need for direct and destructive imaging tools. We have demonstrated this capability in Figure 6A, a typical DF image of individual pyramids on a substrate. After randomly selecting and measuring the spectra of six bright spots (Figure 6B), we found that their spectra fell into two categories: (1) those with 600 nm peaks of relatively high intensity and (2) those with peaks at 600 and 850 nm with comparable intensities. Indeed, when the ratio of scattering intensities at 600 and 850 nm was calculated, two distinct bands emerged (Figure 6C), and SEM images of the pyramids revealed that pyramids with high I_{600}/I_{850} ratios were tip-up and those with low I_{600}/I_{850} ratios were tip-down (Figure 6D).

Effects of Pyramid Shell Thickness on Optical Properties. To determine how the optical properties changed with the thickness (t) of the pyramidal shells, we measured scattering spectra of pyramids with a fixed diameter (d = 300 nm) with t ranging from 15 to 80 nm (Figure 7). Notably, the tip-up and tip-down orientations of thicker pyramids exhibited more pronounced spectral differences than thinner pyramids of the two orientations. For tip-up pyramids, the intensity of the 600 nm peak increased as the thickness of the pyramids increased but seemed to disappear or shift to longer wavelengths, when the thickness decreased. Also, as the thickness of the pyramidal shell approached t = 15 nm, all of the resonances shifted to wavelengths greater than 650 nm (Figure 7D). Thus, besides their ability to support multipolar modes because of size, our pyramidal system can be tuned to exhibit multiple visible and NIR plasmon resonances simply by controlling the thickness of the metal deposition (Figure 1, step C).

In order to investigate the optical properties of gold pyramids at wavelengths longer than 950 nm, we dispersed 300 nm gold particles in D_2O and measured the extinction spectra. Both 60 nm and 110 nm thick pyramids exhibited several resonances between 600 and 1400 nm. In agreement with calculations, as the thickness of the gold pyramid increased, the central resonance was suppressed, and the

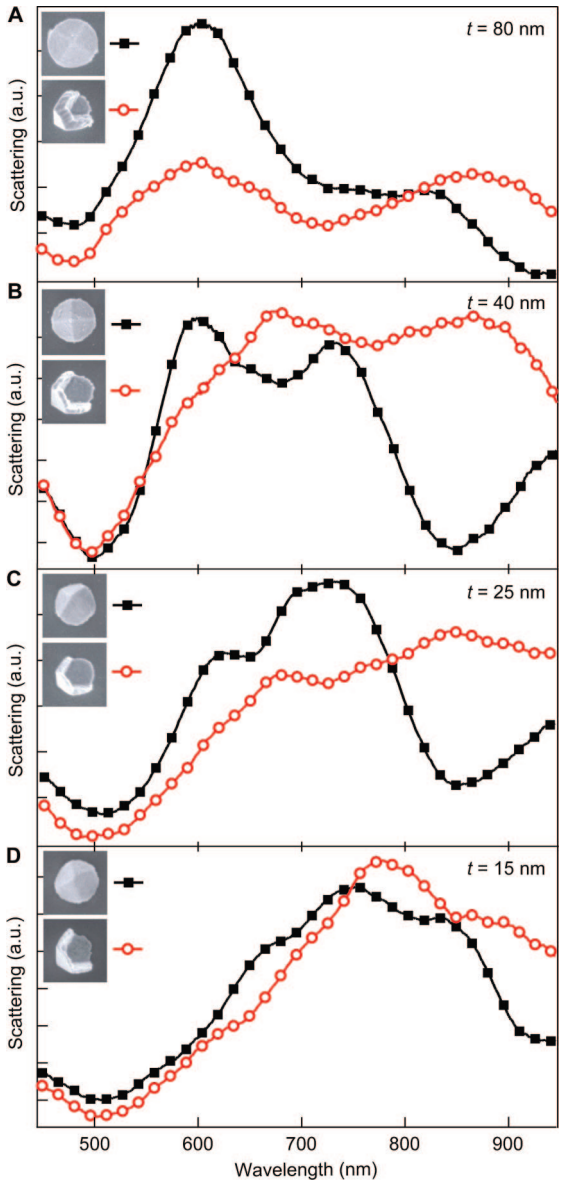

FIGURE 7. Scattering spectra of 300 nm gold pyramids with thicknesses of (A) 80, (B) 40, (C) 25, and (D) 15 nm and with two orientations (tips up (■) and tips down (○)).

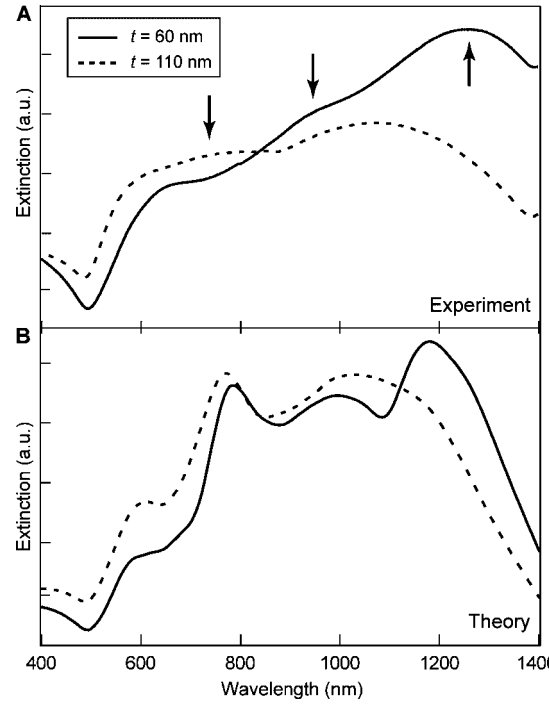

FIGURE 8. (A) Measured and (B) calculated extinction spectra of 60 nm thick (solid line) and 110 nm thick (dashed line) pyramids in D_2O. Modified with permission from ref 51. Copyright 2008 American Chemical Society.

other resonances were shifted to shorter wavelengths (Figure 8).[51] Simulations revealed that the first peak (not the shoulder) was an electric quadrupole resonance and that the third peak was an electric dipole resonance. The most interesting plasmon mode was the one around 1000 nm, which had transverse electric (TE)-like character because of oscillation of the polarization perpendicular to both the incident polarization and wavevector directions. Theory and experiment agree reasonably well on the position of the plasmon mode, but there are some discrepancies in the intensities. This result is expected considering the slight variations in the nanofabricated particles and the extreme sensitivity of extinction with shell thickness. In general, the calculations appear to overestimate the intensity of some resonances, which could be due to factors such as the assumed particle morphology or the chosen dielectric constant at those wavelengths. Overall, however, experiment and theory showed the same trends. In particular, measurements confirmed the three-peak resonance structure that theory predicted for $t = 60$ nm and verified that the central TE-like resonance could be suppressed by increasing the thickness of the pyramids.

Spectroscopic Properties of Arrays of Pyramids

Besides characterizing the optical properties of single pyramids, we were interested in how the SP resonances would evolve as the particles were manipulated into arrays. Studies involving pairs of NPs showed that when the particles are in close proximity, new resonances emerge from plasmon coupling.[52,53] Large field enhancements can also occur between closely spaced particles, which enhances the capability to detect weak interactions such as SERS.[54]

Patterned Two-Dimensional Arrays of Pyramids. The fabrication scheme in Figure 1 allows us to obtain perfectly aligned arrays of gold pyramids that can be encapsulated in an optically transparent polymer. After step C, the anisotropic etching conditions can be controlled such that the pyramids are situated on silicon pedestals. The arrays of pyramids can then be encased in a poly(dimethylsiloxane) (PDMS)

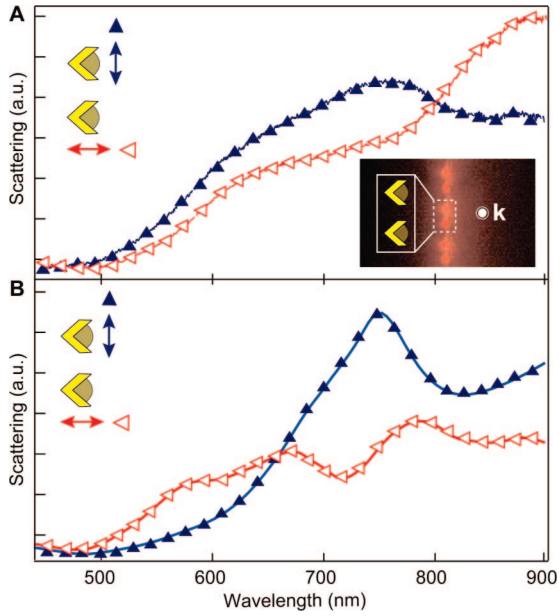

FIGURE 9. (A) Measured and (B) calculated scattering spectra of 250 nm gold pyramid arrays under polarized incident light. Reproduced from ref 11.

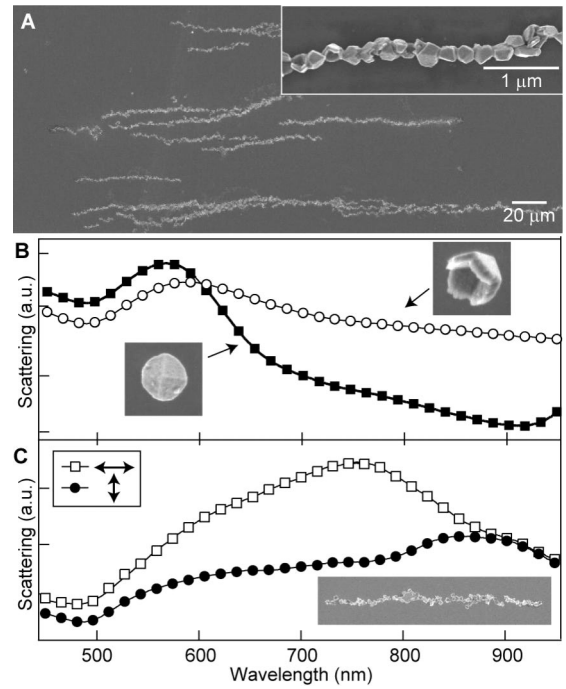

FIGURE 10. (A) SEM image of Au/Ni pyramid chains, (B) scattering spectra of individual Au/Ni pyramids in two orientations, and (C) polarization-dependent scattering spectra of a single Au/Ni chain. Reproduced from ref 46.

matrix to yield a free-standing PDMS membrane. In contrast to pyramids dispersed on a flat substrate, whose orientations are limited to either being tip-up or tip-down (that is, touching the substrate), the PDMS/pyramid film can be placed at an arbitrary angle with respect to the incident light. Because the interparticle distance was too large (ca. 2 μm) for SP coupling between pyramids, the array displayed optical properties similar to that of single pyramids.[45] To investigate the effects of polarization direction, however, we needed to test pyramids in specific, well-defined orientations relative to the DF microscope optical axis; hence, we used aligned 2D arrays.

Not surprisingly, when the base planes of the pyramids were perpendicular to optical axis, the scattering spectra did not show any polarization dependence because the orientation of the pyramids was symmetric with respect to the incident light. When the base planes were oriented parallel to the optical axis, the scattering spectra did exhibit polarization dependence (Figure 9). Rotation of the polarization direction from parallel to perpendicular relative to the pyramid base resulted in a color change from deep-red to light red. Calculations indicated that the plasmon resonance peak under parallel polarization was a quadrupole mode localized in the base plane at 750 nm.[11] Under perpendicular polarization, several resonances emerged with an overall envelope qualitatively similar to the measured result (Figure 9A) except that the intensity of the peak at ca. 880 nm was too weak (Figure 9B).

Assembled One-Dimensional Arrays of Pyramids. Pyramids composed of multiple layers can be easily generated by layer-by-layer deposition of materials (Figure 1, step C). To create bifunctional nanoparticles, we combined the optical properties of gold with the magnetic properties of nickel (Au/Ni pyramids). The ferromagnetism of nickel provides a straightforward means to assemble and manipulate pyramids. Under a static magnetic field (0.5 T), Au/Ni pyramids could be assembled into one-dimensional chains with lengths up to 200 μm (Figure 10A).[46] Orientations of individual nanopyramids within a single chain, however, did not align parallel to the magnetic field lines. As the direction of the magnetic field was rotated, the pyramidal chains also rotated to maintain alignment along field lines.

In chains of Au/Ni pyramids, individual particles were situated very close to each other (less than half of the particle size), which suggests that the plasmon resonances of the pyramids should couple.[55] We measured the scattering spectra of individual 300 nm Au/Ni pyramids and found that (1) there was very little orientation dependence on the optical properties since the peaks at longer wavelengths were suppressed (Figure 10B) and (2) the overall scattering intensities were weaker compared with gold pyramids because nickel dampens the SP resonance of gold.[56] Hence, the different orientations of the pyramids within a chain should not affect the effective properties of the array. Scattering spectra of single Au/Ni pyramid chains depended strongly on polarization of the incident light. Under polarization parallel to the long axis,

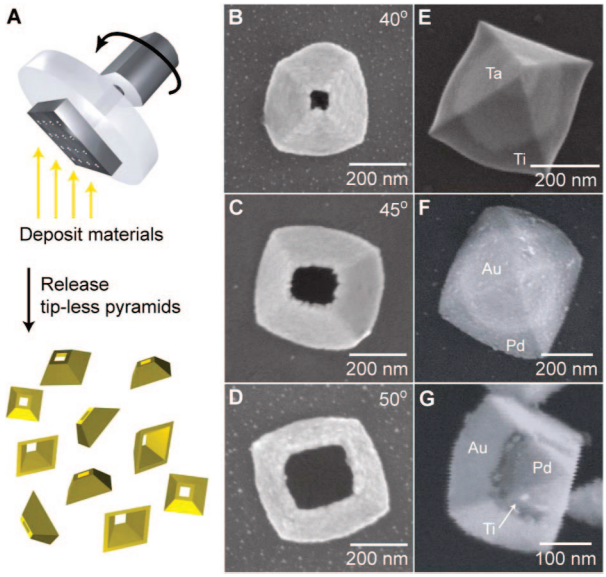

FIGURE 11. (A) Scheme illustrating how the Cr hole/Si etched template can be rotated and tilted at different angles to generate pyramids without tips and with square bases, (B–D) SEM images of tipless gold pyramids deposited at tilt angles of 40°, 45°, and 50°, and SEM images of (E) Ti/Ta pyramidal structure (Ti deposited first at an angle of 45°/Ta deposited at 0°), (F) Pd/Au bimetal pyramidal structure (Pd at 45°/Au at 0°), and (G) Au/Ti/Pd trimetal pyramidal structure (Au at 55°/Ti deposited at 45°/Pd at 0°).

an additional feature at 750 nm was observed, which can be attributed to interparticle SP coupling (Figure 10C).

Expansion of the Platform: Tipless Pyramids

In an effort to address the pressing need for new classes of tunable plasmonic materials, we have developed a method that enables control over particle shape by a creative adaptation of shadow masking techniques. E-beam evaporation of material at a fixed angle relative to a planar template (e.g., photoresist patterns or microspheres[39,40,57]) followed by removal of the template produces a portion or edge of the template but with reduced feature sizes. We have modified our PEEL fabrication scheme to create variations on the pyramidal shape by (1) orienting the Cr hole film/etched Si substrate (after step B) at a range of angles prior to deposition and (2) rotating the sample stage. Figure 11A depicts how the template substrate can be tilted and rotated to generate pyramids without tips and with square bases. Figure 11B–D demonstrates how the angle of the stage can control the size of opening or amount of truncation of the tip. The creation of pyramids with and without tips is particularly interesting for tuning the multipolar plasmon resonances of pyramids; theory has predicted that truncated pyramids should suppress the TE-like resonance mode observed in 300 nm gold pyramids.[51] There are also potential implications for localizing electromagnetic fields at specific locations in tipless pyramids since calculations have already predicted enhancements at the tips and sharp edges of the nanostructures.[11,58]

Multimaterial pyramidal shells whose outer faces are composed of different materials can be obtained by first creating tipless pyramids out of one metal and then depositing a second metal line-of-sight through the Cr hole mask onto the tipless pyramids still embedded in the template. Figure 11E–G highlights a range of pyramidal structures with two or three different metals on the outer faces. This materials tunability is truly unique to the pyramidal system and will enable further opportunities for site-selective chemistry as well as hybridized optical properties of noble metal pyramids.

Conclusions and Outlook

In this Account, we have highlighted how nanofabricated pyramids are a unique platform for designing multifunctional plasmonic particles. Although most research has focused on synthetic methods to create nanoparticles, we believe there are distinct advantages to this optically tunable system: spatial control of chemical and biological moieties; spectral identification of orientation; spatially distinct multimaterial compositions; perfect particle alignment in 2D periodic arrays. In addition, the structure of the pyramidal shells has resulted in unanticipated spectral features, such as TE-like plasmon modes, or has enabled exquisite control over having ultrasharp tips or no tips. Taking into account all capabilities, this class of materials can be considered a leading candidate for biological diagnostics and therapeutic applications.

Besides these applications based on nanoparticles that currently exist, other applications of our pyramidal system that could exist include multifunctional scanning probe microscopy tips for improved spatial resolution as well as magnetic[59] and chemical imaging,[60] inert scaffolds for assembling organic drug particles for delivery applications,[61] and local enhancers of optical absorption in photovoltaic devices.[62] Furthermore, beyond expanding the phase diagram of structure–function relationships for plasmonic particles, we anticipate that our toolkit will offer novel solutions for problems that demand exacting control over structure and composition at the nanometer scale.

This work was supported in part by the Center of Cancer Nanotechnology Excellence initiative of the NIH National Cancer Institute under Award Number U54CA119341, the NSF MRSEC program at Northwestern University (Grant DMR-0520513), NSF Grant DMR-0705741, and the David and Lucile Packard

Foundation. This work used the NUANCE Center facilities, which are supported by NSF-MRSEC, NSF-NSEC, and the Keck Foundation.

BIOGRAPHICAL INFORMATION

Jeunghoon Lee received his B.S. and M.S. degree in Chemical Technology from Seoul National University in 1994 and 1996. He received his Ph.D. in Polymer Science from the University of Connecticut in 2005. After postdoctoral training at Northwestern University under Prof. Teri W. Odom, he joined the Department of Chemistry and Biochemistry at Boise State University. His research interests include the preparation, assembly, and optical applications of inorganic nanoparticles.

Warefta Hasan received a B.S. in Chemistry from the University of Virginia in 2004. She is currently a Ph.D. candidate in Chemistry at Northwestern University. Her research focuses on the fabrication and design of plasmonic nanostructures for biological applications.

Christopher L. Stender received a B.S. in Chemistry from Linfield College in 2002 and is a Ph.D. candidate in Chemistry at Northwestern University. His research interests include synthesis, patterning, and applications of nanostructured materials.

Teri W. Odom is the Dow Professor of Chemistry at Northwestern University. She received her B.S. in Chemistry from Stanford University and her Ph.D. in Chemical Physics from Harvard University. After postdoctoral experience at Harvard University, she joined the Department of Chemistry at Northwestern University and now has a courtesy appointment in Materials Science and Engineering. Her current research focuses on developing and applying large-area nanoscale patterning tools (1) to generate unique plasmonic nanostructures and (2) to facilitate assembly of functional nanomaterials by combining chemistry and fabrication (chemical nanofabrication). Her primary research interests are the optical properties of individual nanostructures and multiscale metal systems such as plasmonic metamaterials.

FOOTNOTES

* To whom correspondence should be addressed. E-mail: todom@northwestern.edu.

REFERENCES

1 Odom, T. W.; Nehl, C. L. How gold nanoparticles have stayed in the light: The 3M's principle. *ACS Nano* **2008**, *2*, 612–616.

2 Xia, Y.; Halas, N. J. Shape-controlled synthesis and surface plasmonic properties of metallic nanostructures. *MRS Bull.* **2005**, *30*, 338–348.

3 Jain, P. K.; Lee, K. S.; El-Sayed, I. H.; El-Sayed, M. A. Calculated absorption and scattering properties of gold nanoparticles of different size, shape, and composition: Applications in biological imaging and biomedicine. *J. Phys. Chem. B* **2006**, *110*, 7238–7248.

4 Rodriguez-Gonzalez, B.; Burrows, A.; Watanabe, M.; Kiely, C. J.; Liz Marzan, L. M. Multishell bimetallic AuAg nanoparticles: Synthesis, structure and optical properties. *J. Mater. Chem.* **2005**, *15*, 1755–1759.

5 Edwards, P. P.; Thomas, J. M. Gold in a metallic divided state-from Faraday to present-day nanoscience. *Angew. Chem., Int. Ed.* **2007**, *46*, 5480–5486.

6 Bohren, C. F.; Huffman, D. R. Absroption and Scattering of Light by Small Particles; Wiley: New York, 1998.

7 Yguerabide, J.; Yguerabide, E. E. Light-scattering submicroscopic particles as highly fluorescent analogs and their use as tracer labels in clinical and biological applications. *Anal. Biochem.* **1998**, *262*, 137–156.

8 Kumbhar, A. S.; Kinnan, M. K.; Chumanov, G. Multipole plasmon resonances of submicron silver particles. *J. Am. Chem. Soc.* **2005**, *127*, 12444–12445.

9 Millstone, J. E.; Park, S.; Shuford, K. L.; Qin, L.; Schatz, G. C.; Mirkin, C. A. Observation of a quadrupole plasmon mode for a colloidal solution of gold nanoprisms. *J. Am. Chem. Soc.* **2005**, *127*, 5312–5313.

10 Shuford, K. L.; Ratner, M. A.; Schatz, G. C. Multipolar excitation in triangular nanoprisms. *J. Chem. Phys.* **2005**, *123*, 114713.

11 Henzie, J.; Shuford, K. L.; Kwak, E.-S.; Schatz, G. C.; Odom, T. W. Manipulating the optical properties of pyramidal nanoparticle arrays. *J. Phys. Chem. B* **2006**, *110*, 14028–14031.

12 Elghanian, R.; Storhoff, J. J.; Mucic, R. C.; Letsinger, R. L.; Mirkin, C. A. Selective colorimetric detection of polynucleotides based on the distance-dependent optical properties of gold nanoparticles. *Science* **1997**, *277*, 1078–1080.

13 Nam, J. M.; Thaxton, C. C.; Mirkin, C. A. Nanoparticles-based bio-bar codes for the ultrasensitive detection of proteins. *Science* **2003**, *301*, 1884–1886.

14 Katz, E.; Willner, I. Integrated nanoparticle-biomolecule hybrid systems: synthesis, properties, and applications. *Angew. Chem., Int. Ed.* **2004**, *43*, 6042–6108.

15 Huang, X.; Jain, P. K.; El-Sayed, I. H.; El-Sayed, M. A. Gold nanoparticles: Interesting optical properties and recent applications in diagnostics and therapy. *Nanomedicine* **2007**, *2*, 789–803.

16 Willets, K. A.; Van Duyne, R. P. Localized surface plasmon resonance spectroscpy and sensing. *Annu. Rev. Phys. Chem.* **2006**, *58*, 267–297.

17 Nie, S. M.; Emory, S. R. Probing single molecules and single nanoparticles by surface-enhanced Raman scattering. *Science* **1997**, *275*, 1102–1106.

18 Haes, A. J.; Haynes, C. L.; McFarland, A. D.; Schatz, G. C.; van Duyne, R. P.; Zou, S. Plasmonic materials for surface-enhanced sensing and spectroscopy. *MRS Bull.* **2005**, *30*, 368–375.

19 Loo, C.; Lowery, A.; Halas, N. J.; West, J. L.; Drezek, R. Immunotargeted nanoshells for integrated cancer imaging and therapy. *Nano Lett.* **2005**, *5*, 709–711.

20 Hirsch, L. R.; Stafford, R. J.; Bankson, J. A.; Sershen, S. R.; Rivera, B.; Price, R. E.; Hazle, J. D.; Halas, N. J.; West, J. L. Nanoshell-mediated near-infrared thermal therapy of tumors under magnetic resonance guidance. *Proc. Natl. Acad. Sci. U.S.A.* **2003**, *100*, 13549–13554.

21 Huang, X.; El-Sayed, I. H.; Qian, W.; El-Sayed, M. A. Cancer cell imaging and photothermal therapy in the near-infrared region by using gold nanorods. *J. Am. Chem. Soc.* **2006**, *128*, 2115–2120.

22 Goodman, C. M.; McCusker, C. D.; Yilmaz, T.; Rotello, V. M. Toxicity of gold nanoparticles functionalized with cationic and anionic side chains. *Bioconjugate Chem.* **2004**, *15*, 897–900.

23 Lee, K. J.; Nallathamby, P. D.; Browning, L. M.; Osgood, C. J.; Xu, X. H. N. In vivo imaging of transport and biocompatibility of single silver nanoparticles in early development of zebrafish embryos. *ACS Nano* **2007**, *1*, 133–143.

24 Link, S.; El-Sayed, M. A. Shape and size dependence of radiative, non-radiative and photothermal properties of nanocrystals. *Int. Rev. Phys. Chem.* **2000**, *19*, 409–453.

25 Govorov, A. O.; Richardson, H. H. Generating heat with metal nanoparticles. *Nanotoday* **2007**, *2*, 30–38.

26 Murphy, C. J.; Sau, T. K.; Gole, A. M.; Orendorff, C. J.; Gao, J.; Gou, L.; Hunyadi, S. E.; Li, T. Anisotropic metal nanoparticles: synthesis, assembly, and optical applications. *J. Phys. Chem. B* **2005**, *109*, 13857–13870.

27 Xia, Y. J.; Yang, P.; Sun, Y.; Wu, Y.; Mayers, B.; Gates, B.; Yin, Y.; Kim, F.; Yan, H. One-dimensional nanostructures: Synthesis, characterization, and applications. *Adv. Mater.* **2003**, *15*, 353–389.

28 Sherry, L. J.; Chang, S.-H.; Schatz, G. C.; Van Duyne, R. P.; Wiley, B. J.; Xia, Y. Localized surface plasmon resonance spectroscopy of single silver nanocubes. *Nano Lett.* **2005**, *5*, 2034–2038.

29 Chen, J.; McLellan, J. M.; Siekkinen, A.; Xiong, Y.; Li, Z. Y.; Xia, Y. J. Facile synthesis of gold-silver nanocages with controllable pores on the surface. *J. Am. Chem. Soc.* **2006**, *128*, 14776–14777.

30 Jin, R.; Cao, Y.; Mirkin, C. A.; Kelly, K. L.; Schatz, G. C.; Zheng, J. G. Photoinduced conversion of silver nanospheres to nanoprisms. *Science* **2001**, *294*, 1901–1903.

31 Nehl, C. L.; Liao, H.; Hafner, J. H. Optical properties of star-shaped gold nanoparticles. *Nano Lett.* **2006**, *6*, 683–688.

32 Tao, A.; Sinsermsuksakul, P.; Yang, P. Polyhedral silver nanocrustals with distinct scattering signatures. *Angew. Chem., Int. Ed.* **2006**, *45*, 4597–4601.

33 Yu, H.; Chen, M.; Rice, P. M.; Wang, S. X.; White, R. L.; Sun, S. Dumbbell-like bifunctional Au-Fe_3O_4 nanoparticles. *Nano Lett.* **2005**, *5*, 379–382.

34 Xu, X.; Rosi, N. L.; Wang, Y.; Huo, F.; Mirkin, C. A. Asymmetric functionalization of gold nanoparticles with oligonucleotides. *J. Am. Chem. Soc.* **2006**, *128*, 9286–9287.

35 Sardar, R.; Heap, T. B.; Shumaker-Parry, J. S. Versatile solid phase synthesis of gold nanoparticle dimers using an asymmetric functionalization approach. *J. Am. Chem. Soc.* **2007**, *129*, 5356–5357.

36 DeVries, G. A.; Brunnbauer, M.; Hu, Y.; Jackson, A. M.; Long, B.; Neltner, B. T.; Uzun, O.; Wunsch, B. H.; Stellacci, F. Divalent metal nanoparticles. *Science* **2007**, *315*, 358–361.

37 Canfield, B. K.; Kujala, S.; Kauranen, M.; Jefimovs, K.; Vallius, T.; Turunen, J. Remarkable polarization sensitivity of gold nanoparticle arrays. *Appl. Phys. Lett.* **2005**, *86*, 183109.

38 Hicks, E. M.; Zou, S.; Schatz, G. C.; Spears, K. G.; Van Duyne, R. P.; Gunnarson, L.; Rindzevicius, T.; Kasemo, B.; Kall, M. Controlling plasmon line shapes through diffractive coupling in linear arrays of cylindrical nanoparticles fabricated by electron beam lithography. *Nano Lett.* **2005**, *5*, 1065–1070.

39 Shumaker-Parry, J. S.; Rochholz, H.; Kreiter, M. Fabrication of crescent-shaped optical antennas. *Adv. Mater.* **2005**, *17*, 2131–2134.

40 Liu, G. L.; Lu, Y.; Kim, J.; Doll, J. C.; Lee, L. P. Magnetic nanocrescents as controllable surface-enhanced raman scattering nanoprobe for biomolecular imaging. *Adv. Mater.* **2005**, *17*, 2683–2688.

41 Haes, A. J.; Zhao, J.; Zou, S.; Own, C. S.; Marks, L. D.; Schatz, G. C.; Van Duyne, R. P. Solution-phase, triangular Ag nanotriangles fabricated by nanosphere lithography. *J. Phys. Chem. B* **2005**, *109*, 11158–11162.

42 Nicewarner-Pena, S. R.; Freeman, R. G.; Reiss, B. D.; He, L.; Pena, D. J.; Walton, I. D.; Cromer, R.; Keating, C. D.; Natan, M. J. Submicrometer metallic barcodes. *Science* **2001**, *294*, 137–141.

43 Henzie, J.; Kwak, E.-S.; Odom, T. W. Mesoscale metallic pyramids with nanoscale tips. *Nano Lett.* **2005**, *5*, 1199–1202.

44 Xu, Q.; Tonks, I.; Fuerstman, M. J.; Love, J. C.; Whitesides, G. M. Fabrication of free-standing metallic pyramidal shells. *Nano Lett.* **2004**, *4*, 2509–2511.

45 Hasan, W.; Lee, J.; Henzie, J.; Odom, T. W. Selective functionalization and spectral identification of Au nanopyramids. *J. Phys. Chem. C* **2007**, *111*, 17176–17179.

46 Lee, J.; Hasan, W.; Lee, M. H.; Odom, T. W. Optical properties and magnetic manipulation of bi-material nanopyramids. *Adv. Mater.* **2007**, *19*, 4387–4391.

47 Krenn, J. R.; Schider, G.; Rechberger, W.; Lamprecht, B.; Leitner, A.; Aussenegg, F. R.; Weeber, J. C. Design of multipolar plasmon excitations in silver nanoparticles. *Appl. Phys. Lett.* **2000**, *77*, 3379–3381.

48 Payne, E. K.; Shuford, K. L.; Park, S.; Schatz, G. C.; Mirkin, C. A. Multipole plasmon resonances in gold nanorods. *J. Phys. Chem. B* **2006**, *110*, 2150–2154.

49 Oldenburg, S. J.; Hale, G. D.; Jackson, J. B.; Halas, N. J. Light scattering from dipole and quadrupole nanoshell antennas. *Appl. Phys. Lett.* **1999**, *75*, 1063–1065.

50 Kelly, K. L.; Coronado, E.; Zhao, L. L.; Schatz, G. C. The optical properties of metal nanoparticles: The influence of size, shape, and dielectric environment. *J. Phys. Chem. B* **2003**, *107*, 668–677.

51 Shuford, K. L.; Lee, J.; Odom, T. W.; Schatz, G. C. Optical properties of gold pyramidal shells. *J. Phys. Chem. C* **2008**, *112*, 6662–6666.

52 Atay, T.; Song, J.-H.; Nurmikko, A. V. Strongly interacting plasmon nanoparticle pairs: From dipolar interaction to conductively coupled regime. *Nano Lett.* **2004**, *4*, 1627–1631.

53 Lassiter, J. B.; Aizpurua, J.; Hernandez, L. I.; Brandl, D. W.; Romero, I.; Lal, S.; Hafner, J. H.; Nordlander, P.; Halas, N. J. Close encounters between two nanoshells. *Nano Lett.* **2008**, *8*, 1212–1218.

54 Svedberg, F.; Li, Z.; Xu, H.; Kall, M. Creating hot nanoparticle pairs for surface-enhanced Raman spectroscopy through optical manipulation. *Nano Lett.* **2006**, *6*, 2639–2641.

55 Lin, S.; Li, M.; Dujardin, E.; Girard, C.; Mann, S. One-dimensional plasmon coupling by facile self-assembly of gold nanoparticles into branched chain networks. *Adv. Mater.* **2005**, *17*, 2553–2559.

56 Gaudry, M.; Cottancin, E.; Pellarin, M.; Lerme, J.; Arnaud, L.; Huntzinger, J. R.; Vialle, J. L.; Broyer, M. Size and composition dependence in the optical properties of mixed (transition metal/noble metal) embedded clusters. *Phys. Rev. B* **2003**, *67*, 155409.

57 Gates, B.; Xu, Q.; Thalladi, V. R.; Cao, T.; Knickerbocker, T.; Whitesides, G. M. Shear patterning of microdominos: A new class of procedures for making micro- and nano-structures. *Angew. Chem., Int. Ed.* **2004**, *43*, 2780–2783.

58 Hao, E.; Schatz, G. C. Electromagnetic fields around silver nanoparticles and dimers. *J. Chem. Phys.* **2004**, *120*, 357–366.

59 Mamin, H. J.; Poggio, M.; Degen, C. L.; Rugar, D. Magnetic resonance imaging with 90-nm resolution. *Nat. Nanotechnol.* **2007**, *2*, 301–306.

60 Noy, A. Strength in numbers: Probing and understanding intermolecular bonding with chemical force microscopy. *Scanning* **2008**, *30*, 96–105.

61 Han, G.; Ghosh, P.; Rotello, V. M. Functionalized gold nanoparticles for drug delivery. *Nanomedicine* **2007**, *2*, 113–123.

62 Pillai, S.; Catchpole, K. R.; Trupke, T.; Green, M. A. Surface Plasmon Enhanced Silicon Solar Cells. *J. Appl. Phys.* **2007**, *101*, 093105.